# X-ray structural analysis of compensating mutations at the barnase-barstar interface

Carole Martin[a], Robert Hartley[b], Yves Mauguen[a,*]

[a] *Laboratoire de Physique, Centre d'Etudes Pharmaceutiques, rue JB, Clément, 92296 Châtenay-Malabry Cedex, France*
[b] *Laboratory of Cellular and Developmental Biology, National Institute of Diabetes and Digestive and Kidney Diseases, National Institute of Health, Bethesda, MD 20892, USA*

Received 2 February 1999; received in revised form 22 April 1999

**Abstract The crystal structure of the barstar mutants (Y29P) and (Y29D, Y30W) as well as that of the complexes of barstar(Y29P) with wild-type barnase and barnase(H102K) have been determined. These barstar mutants compensate for the dramatic loss of barnase-barstar interaction energy caused by a single mutation of the barnase active site His-102 to a lysine. The latter introduces an uncompensated charge in the pocket at the surface of barstar where Lys-102 is located. The analysis of the structures suggests a mechanism for this compensation based on the solvation of the charge of Lys-102. Additional compensation occurs through the formation of a hydrogen bond.**



*Key words:* Protein-protein recognition; Compensating mutation; RNase-inhibitor complex; X-ray crystallography

## 1. Introduction

One of the tightest and fastest protein-protein interactions known is the interaction between a small extracellular ribonuclease from *Bacillus amyloliquefaciens* (barnase) [1] and its natural intracellular inhibitor (barstar) [2]. The inhibition involves the formation of a tight one to one non-covalent complex of the two proteins ($K_d = 1.3 \times 10^{-14}$ M) [3,4].

The barnase and barstar structures have both been determined by X-ray crystallography [5,6] and by NMR [7,8]. The crystal structure of the complex of barnase with barstar is also known [9,10]. Barstar inhibits barnase by sterically blocking the active site. The structures of the two proteins in the barnase-barstar complex are almost identical to the uncomplexed structures [6,11]. The barnase residues involved in the protein/protein interface are mostly in the active site and in the recognition loop of the enzyme. The part of barstar involved in the inhibitory function consists of a continuous polypeptide fragment (residues 29–46), which comprises a short α-helix and a loop.

To study the interaction between barnase and barstar, suppressor mutations in barstar that compensate for the loss in interaction energy caused by a mutation in barnase were isolated through a genetic screen in vivo [12]. The barnase mutant with the catalytic residue substitution H102K retains a weak residual ribonuclease activity that is not properly inhibited by the wild-type barstar [13]. The six residues of barstar that contact barnase His-102 in the native complex (Fig. 1) were randomly mutagenized. Two mutants, (Y29P) and (Y30W), provided a better protection against the ribonuclease activity of barnase(H102K). The barstar(Y29D, Y30W) double mutant was the overall best suppressor. Whereas the dissociation constant of the barnase(H102K)-barstar complex is about $10^{-5}$ M, that of the barnase(H102K)-barstar(Y29D, Y30W) complex is $10^{-9}$ M [12].

We report here the crystal structure of the barstar(Y29P) mutant both in the free form and complexed with wild-type barnase and with barnase(H102K), as well as the crystal structure of the uncomplexed barstar(Y29D, Y30W) double mutant. These provide rationales for the compensating effects of these mutations in the barnase-barstar interface.

## 2. Materials and methods

### 2.1. Proteins

Wild-type barnase and barnase(H102K) were expressed in XL1-blue *Escherichia coli* containing the plasmid pMJ1002 or in D1210 *E. coli* harboring the recombinant plasmid pMJ2, respectively [12,13]. Barstar has two cysteines at positions 40 and 82. The heterogeneity of the oxidation state and the tendency of the two cysteines to form mixed disulfides, dimers and multimers, have hampered attempts to crystallize wild-type barstar. For this reason, all barstar molecules in crystal structures reported here have the two cysteines replaced by alanine. The barstar(C40A, C82A) double mutant binds barnase with a dissociation constant very similar to that of wild-type barstar and is being used as a pseudo wild-type [3]. Barstar mutants (Y29P, C40A, C82A) and (Y29D, Y30W, C40A, C82A) were overexpressed in *E. coli* strain HB101 harboring plasmids pMJ110 or pMJ104, respectively [12]. Proteins were purified mostly in the same way as their wild-type homologs [14–16]. Complexes were prepared by mixing barnase and barstar in an equimolar ratio. Concentrations of mutant solutions were determined by measuring the absorption at 280 nm using extinction coefficients estimated by the method of Gill and von Hippel [17].

### 2.2. Crystallization and X-ray data collection

Crystallizations used the hanging drop method at room temperature (18–20°C) in Linbro tissue culture plates. Barstar mutant crystals were grown from a protein solution (15 mg/ml) in 50 mM Tris-HCl buffer, pH 8, mixed in a 1:1 ratio with 1.1–1.3 M phosphate potassium buffer, pH 8, for barstar(Y29P) or 1.25 M sodium citrate, 0.1 M Tris-HCl buffer, pH 8, for barstar(Y29D, Y30W). These crystallization conditions are similar to those used to crystallize wild-type barstar [9,18]. Crystals of the barnase-barstar(Y29P) complex were obtained from a 10 mg/ml protein solution in 50 mM Tris-HCl buffer, pH 8, mixed in a 1:1 ratio with 3% PEG4000, 10% DMSO in the same buffer. Barnase(H102K)-barstar(Y29P) crystallizes from a solution of the complex (14 mg/ml) in 50 mM Tris-HCl buffer, pH8, mixed with an equal volume of 2.4 M ammonium sulfate in the same buffer. In the last case, macro seeding was used to improve the crystal size [19].

X-ray diffraction data were collected at 4°C from a single crystal of each species, on the wiggler line W32 at LURE (Université Paris-Sud Orsay) using a wavelength of 0.97 Å and a MAR Research imaging

*Corresponding author. Fax: (33) (1) 46 83 56 30.
E-mail: yves.mauguen@cep.u-psud.fr

0014-5793/99/$20.00 
PII: S0014-5793(99)00621-3

plate scanner. Data were processed using the MOSFLM package [20], statistics are reported in Table 1.

*2.3. Structure determination*

The four structures reported here were solved by molecular replacement using the AMoRe suite of programs [21,22]. Rotation and translation functions were calculated over the 15–3.5 Å resolution range. The barnase-barstar structure (file names 1BRS and 1BGS in the Protein Data Bank) provided the search models for all the structures. In the barnase-barstar crystals [9,10] as well as in barstar crystals [6], barstar molecules form dimers. In these, the last strand of the three stranded parallel β-sheet of one molecule hydrogen bonds to the same β-strand in the second monomer of the dimer in an anti-parallel β-sheet fashion. This dimer was used as a model to determine the structure of the two barstar mutants studied here. In these cases, rigid body refinement led to an R-factor of 45.6% at 3.5 Å for barstar-(Y29P) and of 41.8% for barstar(Y29D, Y30W). The barnase-barstar complex was used as a search model for the barnase-barstar(Y29P) structure. In this case, the R-factor was 34.3% after rigid body refinement. The structure of the barnase(H102K)-barstar(Y29P) complex, with six complexes in the asymmetric unit, was solved using the Cα backbone of a dimer of complexes [9] as a model. Rigid body refinement of complete models of the six complexes led to an R-factor of 46.5%. After a rotation search, three translation functions were computed successively, each taking into account the models positioned in previous steps [22]

*2.4. Refinement and structure analysis*

The molecular models were structurally optimized by alternate cycles of positional refinement by simulated annealing or conjugate gradient minimization, of restrained individual B-factor refinement and of model building in difference Fourier maps. All the re-building was performed using the program packages TURBO-FRODO [23] and O [24]. Refinements were performed with the program X-PLOR [25]. The bond length and angle parameters used were those of Engh and Huber [26]. The mutated residues were modelled during the first round of map inspection. Solvent molecules were added (i) if they were in well-defined (3Fo-2Fc) and (Fo-Fc) electron density, above the 1σ and 3σ levels, respectively, and (ii) if they established stereochemically acceptable hydrogen bonds with protein atoms or with solvent molecules previously incorporated in the model. In the case of the barnase(H102K)-barstar(Y29P) complex, refinement was constrained by the non-crystallographic symmetry relating the six independent complexes of the asymmetric unit and two group B-factors were refined per residue, one for the backbone atoms (Cα, N, C and O) and one for the side-chain. In all cases, the stereochemistry of the models was assessed with the program PROCHECK [27]. Structural comparisons were made using the program LSQKAB in the CCP4 package [28].

## 3. Results and discussion

*3.1. Quality of the structures*

(i) The mutant structures barstar(Y29P) and barstar(Y29D, Y30W) have been determined at a 2.2 Å resolution and that of the complex of barstar(Y29P) with barnase at 2.1 Å. In these three crystallographic structures, there are two molecules (barstar or complex) in the asymmetric unit, which improve the accuracy of the resulting atomic models. Least squares superimposition of the Cα atoms of the two independent molecules in each structure gives Cα root mean square (rms) deviations of 0.52, 0.27 and 0.21 Å, respectively. R-factors are 0.180, 0.166 and 0.154, respectively, and the stereochemistry is within the range expected at such a resolution (Table 1). The high accuracy of these structures is confirmed by the Ramachandran plots for each structure, using PROCHECK [29], with no residue in non-allowed (φ, ι) regions and by average errors of coordinates ranging from 0.20 to 0.25 Å, as estimated from Luzzati plots [30]. For barstar-(Y29P) structures, there is a continuous density at the N-terminal extremity indicating the presence of the N-terminal methionine residue, which is not split off when barstar is overexpressed in *E. coli* [31]. The side-chain of this methionine residue was included with the partial occupancy factor (0.5) in molecules A and B of the barstar(Y29P) structure, likewise side-chain atoms of the Lys-1 residue of molecule B. The two high resolution structures of barstar(Y29P), free and complexed with barnase, clearly demonstrate that the peptide conformation at Pro-29 is *cis*. In the barstar(Y29D, Y30W) double mutant, substitution at position 30 fits the electron density consistently, but the Asp-29 residue and the Glu-28 side-chain appear to be disordered, with a discontinuous density in an (2Fo-Fc) electron density map contoured at 0.8σ.

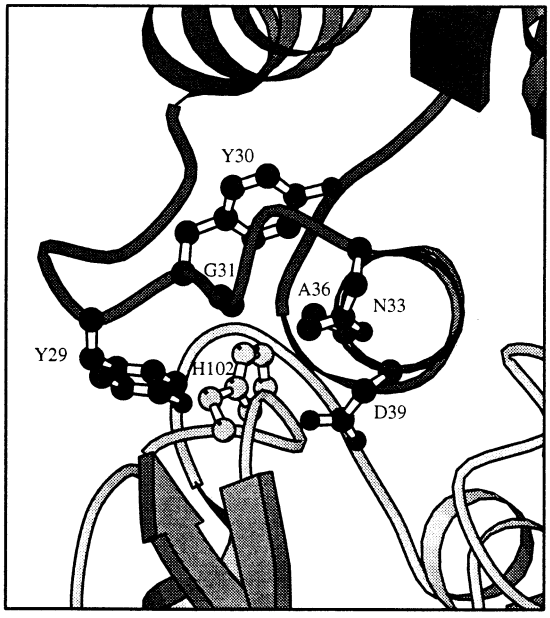


Fig. 1. Active site His-102 of barnase and its barstar environment. The side-chain of His-102 fits into the surface barstar pocket defined by residues Tyr-29, Tyr-30, Gly-31, Asn-33, Ala-36 and Asp-39.

(ii) The structure of the barnase(H102K)-barstar(Y29P) complex was determined at a 3.0 Å resolution. This structure comprises six complexes in the asymmetric unit. The stereochemistry (Table 1) is conforming to the standard at this resolution. 87% of the residues are within the most favored regions of the Ramachandran plot and the only five residues (0.5%) in disallowed regions are the Asn-65 of barstar molecules, located in a flexible loop. The rms deviations between the six complexes related by non-crystallography symmetry is about 0.3 Å for all the non-H atoms. Average B-factors range from 11.5 to 15 $Å^2$ for the six independent complexes and the following analysis relates to the best defined complex.

*3.2. Structural effects of barstar Y29P and (Y29D, Y30W) mutations*

The overall fold of the barstar(Y29P) and barstar(Y29D, Y30W) mutants closely resembles that of the wild-type. rms differences of all the barstar structures (wild-type or mutant, free or barnase-complexed) after a least squares fit of all the Cα atoms range from 0.21 to 0.71 Å. A comparison of the deviations highlights the disorder of residues 60–66 and the flexibility of the part of barstar important for the inhibitory function named the recognition loop. This consists of a con-

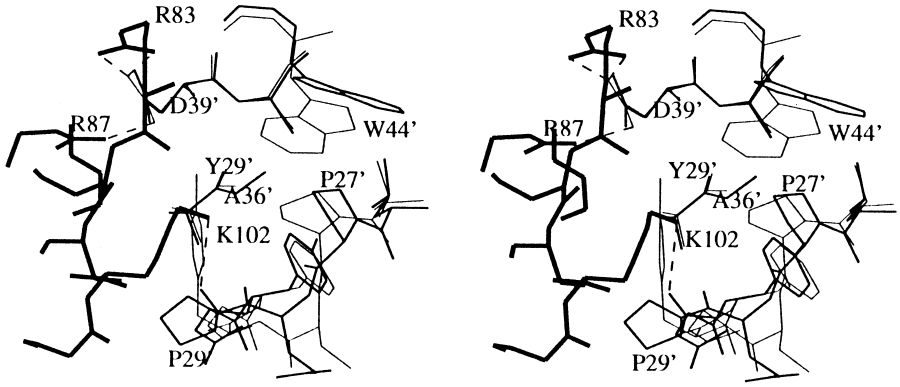


Fig. 2. Stereoscopic view of complexes built by superimposing the barnase(H102K)-barstar(Y29P) complex onto the wild-type barnase-barstar complex followed by the removal of the wild-type barnase. Barstar residues are labelled with a '. Barnase(H102K): thick line; barstar: thin line; barstar(Y29P): medium line.

tinuous polypeptide fragment (residues 29–46) which corresponds to a short helix (residues 33–44) and to a loop. The large temperature factors of these residues are consistent with the flexibility revealed by the NMR structure of barstar [8]. They decrease upon complexation with barnase. Despite this flexibility, the conformation of the residues involved in the binding of barstar to barnase is clearly defined, in particular the *cis* Pro-29 of barstar(Y29P) and the Trp-30 side-chain of barstar(Y29D, Y30W).

### 3.3. *Why does the barnase mutation H102K dramatically decrease the affinity between barnase and barstar?*

His-102 is one of the major contributors to the buried surface area in the barnase-barstar interface, with 110 Å$^2$ out of a total of 803 Å$^2$ of the barnase surface buried in the complex corresponding to this residue [10]. Residue His-102 establishes three hydrogen bonds to barstar through its side-chain and carbonyl oxygen. The His-102 side-chain also interacts face to edge with the aromatic ring of barstar Tyr-29 and fits into a pocket at the surface of barstar delineated by residues Tyr-29, Tyr-30, Gly-31, Asn-33, Ala-36 and Asp-39 (Fig. 1).

Detailed protein engineering studies on the interaction of barnase and barstar have revealed the contributions of specific residues to the free energy and kinetics of binding and in particular those of His-102 and of the residues that interact with it in the barnase-barstar interface [4]. The single mutation H102A results in a loss ($\Delta\Delta G$) of 6.1 kcal/mol binding energy whereas mutation to Asp or Gln resulted in a smaller loss of 4.5 kcal/mol [3]. While the H102A mutation disrupts two hydrogen bonds with barstar, the Asp or Gln mutant residues can be modelled in conformations such that one of the His-102 hydrogen bonds with barstar is retained, without introducing any steric clash [10]. Residue Tyr-29 of barstar is one of those that contact His-102 of barnase. Its mutation to Ala results in a loss of 3.4 kcal/mol binding energy. The pair Tyr-29/His-102 has a coupling energy of 3.3 kcal/mol, which cannot be explained simply as a base to aromatic interaction [32].

Table 1
Results of crystallographic data processing and structure refinement

| | Barstar(Y29P) | Barnase-barstar(Y29P) complex | Barnase(H102K)-barstar(Y29P) complex | Barstar(Y29D, Y30W) |
|---|---|---|---|---|
| Space group | $P2_1$ | $P6_3$ | $P3_221$ | $P6_1$ |
| Cell dimensions: a, b, c (Å) | 50.94, 37.70, 52.46 | 70.89, 70.89, 153.09 | 110.16, 110.16, 210.15 | 59.4, 59.4, 116.9 |
| Angle | $\beta = 99.5°$ | $\gamma = 120°$ | $\gamma = 120°$ | $\gamma = 120°$ |
| Independent molecules | 2 | 2 | 6 | 2 |
| Resolution | 2.1 Å | 2.2 Å | 3.0 Å | 2.2 Å |
| Collected reflections | 43 280 | 104 913 | 158 695 | 38 027 |
| Unique reflections | 11 659 | 22 039 | 30 199 | 9 105 |
| Data completeness | 99.7% | 99.6% | 99.7% | 77.4% |
| R*sym* | 4.5% | 8.1% | 12.9% | 6.1% |
| Refined model | | | | |
| R-factor | 18.0% | 15.4% | 23.3% | 16.6% |
| Resolution range | 7–2.1 Å | 10–2.2 Å | 10–3.0 Å | 7–2.2 Å |
| Model: | | | | |
| Number of non-H atoms | 1 432 | 3 160 | 9 426 | 1 424 |
| Number of waters | 92 | 340 | 90 | 89 |
| rms deviations: | | | | |
| Covalent bond lengths | 0.016 Å | 0.013 Å | 0.018 Å | 0.014 Å |
| Bond angles | 2.010° | 1.651° | 2.132° | 1.694° |
| Average B-factor (Å$^2$): | | | | |
| For the barstar molecules: | 26.2, 35.5 | 14.7, 15.0 | from 11.5 to 15. | 39.0, 38.9 |
| For the water molecules: | 45.7 | 34.2 | 15.0 | 55.4 |

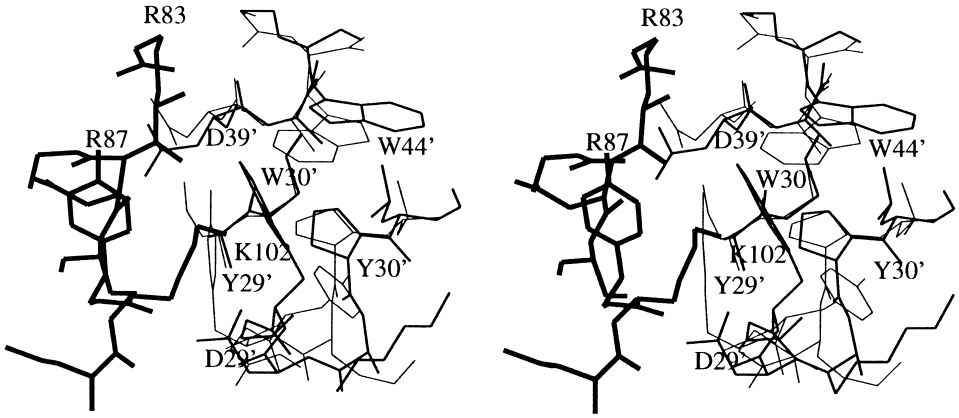


Fig. 3. Stereoscopic view of artificial complexes built by superimposing onto the wild-type complex, both the uncomplexed barstar(Y29D, Y30W) and the barnase(H102K) taken from the barnase(H102K)-barstar(Y29P) complex, followed by the removal of the wild-type barnase. Barstar residues are labelled with a '. Barnase(H102K): thick line; barstar: thin line; barstar(Y29D, Y30W): medium line.

The value of the dissociation constant, $K_d$, of the complex of barnase and barstar corresponds to a −18.9 kcal/mol $\Delta G$ [3,4]. The dissociation constant of the complex of barnase(H102K) with wild-type barstar is about $10^{-5}$ M, nine orders of magnitude greater than the dissociation constant of wild-type complex and corresponds to a $\Delta\Delta G$ of 13 kcal/mol [12]. This is significantly larger than the effects of previously described mutations in the barnase-barstar interface. To analyze the possible causes for this large effect, a model of the barnase(H102K)-barstar complex structure was generated by replacing in the wild-type barnase-barstar complex the His-102 residue by the corresponding lysine in its conformation observed in the barnase(H102K)-barstar(Y29P) complex. Two direct effects of the mutation have been identified. Firstly, the H102K mutation disrupts the two hydrogen bonds established by side-chain atoms of His-102 with barstar. Secondly, owing to the size of the lysine side-chain, this residue would produce unfavorable interactions with barstar which require a modification of the Tyr-29 side-chain conformation. This in turn would disrupt the two hydrogen bonds to barnase atoms made by the barstar Tyr-29 OH group in the wild-type complex.

In addition to the effect of the H102K mutation on the direct barnase-barstar atomic interactions, there is a destabilizing effect of the positive charge of the substituted lysine. It has been shown that the p$K_a$ of His-102, equal to 6.3 in wild-type barnase, is lowered to less than 5.0 in the barnase-barstar complex [4]. This variation of p$K_a$ is explained by the structure of the native complex where the ND1 of barnase His-102 forms a hydrogen bond with the NH of barstar Gly-31, which can occur only when the imidazole group is unprotonated [9,10]. Therefore, the H102K mutation introduces a positive charge in the catalytic site of barnase located in a depression at the surface of the β-sheet, where three positively charged residues (Arg-83, Arg-87, Lys-27) are buried and cause electrostatic strain. The extent of this strain is suggested by a small but definite stabilizing effect of the mutation to alanine of several of the positively charged residues on the barnase surface [33]. Some of this strain is released in the barnase-barstar complex through the hydrogen bonds of barstar residue Asp-39 with Arg-83, Arg-87 and His-102 of barnase, but this aspartic acid residue cannot compensate for the additional positive charge introduced in the interface by the H102K mutation.

### 3.4. How do barstar mutants restore the barnase(H102K) inhibition?

(1) Barstar(Y29P). A superimposition of the barstar(Y29P) mutant structure onto the wild-type barstar complexed with barnase is shown in Fig. 2. This shows that the Y29P mutation causes significant shifts of inhibitor residues close to the mutation site which result in a wider opening of the surface barstar pocket where barnase Lys-102 is located. This opening may be monitored by calculating accessible surface areas. The side-chain of His-102, with a solvent accessible surface of 13 and 15 Å$^2$ in the two independent complexes in the barnase-barstar(Y29P) structure, is more accessible than in the wild-type complex structure, where its solvent accessible surface is 1 Å$^2$. The accessible surface of Lys-102 in the barnase-(H102K)-barstar(Y29P) complex is even larger (20 Å$^2$) and this allows its solvation by surrounding water. In addition, the *cis* conformation of the Pro-29 residue allows the formation of a hydrogen bond between its carbonyl group and the NZ atom of Lys-102, thus increasing the stability of the complex of barstar(Y29P) with barnase(H102K). The limited resolution (3 Å) of this structure has not allowed to detect water molecules bound to Lys-102 with confidence. The solvent accessible volume of the cavity created by the mutations was calculated with the program VOIDOO [34] and found to be equal to 19 Å$^3$ with a S.D. of 4 Å$^3$. Using the program FLOOD [34], it was estimated that the size of such a cavity was large enough to accommodate 7–9 water molecules without steric clash with neighboring atoms and potential hydrogen bonding of some of them with the NZ of Lys-102.

(2) Barstar(Y29D, Y30W). In the wild-type complex, the phenolic group of Tyr-30 is completely buried in the barstar structure and contacts barnase solely through its peptide backbone. In the mutant, the indole group flips out and becomes exposed to the solvent while the overall conformation of the barstar recognition loop is conserved (Fig. 3). A water molecule occupies the space left void by the flipped out Trp-30 side-chain. The Trp-44 side-chain moves too and this contributes to the opening of the barstar pocket where barnase residue 102 is located. The barstar Y30W mutation would there-

fore indirectly facilitate solvation of the charge of the Lys-102 residue of mutated barnase. An additional effect is suggested by the model of the barstar(Y29D, Y30W) complexed with barnase(H102K) that results from replacing the barstar(Y29P) in its complex with barnase(H102K) by the double mutant structure. In this model, the indole side-chain at position 30 makes unfavorable contacts with the Lys-102. The simplest way to remove them will require a displacement of the Lys-102 side-chain. The opening of the cavity where this lysine is located allows it to project into the solvent. The negatively charged Asp-29 of the mutant barstar would then be in a position to establish a salt bridge with the Lys-102 side-chain.

Compensating mutations (Y29P) and (Y29D, Y30W) induce extremely localized changes in the barstar structure rather than overall changes of the complex. Despite very different affinities ($10^{-14}$ versus $10^{-9}$ M), buried surfaces in the wild-type or the barnase(H102K)-barstar(Y29D, Y30W) complexes are very similar (1590 Å$^2$ versus 1565 Å$^2$). The structure of the barnase(H102K)-barstar(Y29P) complex shows that the mutation allows hydration of the positive charge of Lys-102 as well as a partial compensation of this charge through a hydrogen bond with the carbonyl oxygen of Pro-29. Similar interpretations result from the model of the complex of barstar(Y29D, Y30W) with barnase(H102K) that is based on the structure of the uncomplexed mutant.

The substitution of the barnase His-102 by a lysine decreases the barnase-barstar association constant by introducing an uncompensated positive charge at the interface. It may therefore seem paradoxical that the most efficient compensating mutation of residue 29 of barstar, which is the most solvent accessible of those that bury barnase His-102, is not to a negatively charged residue. Results of the effect of mutations of barstar on its stability provide a possible explanation. Mutation to alanine of one of the two aspartic acid chains of barstar fully exposed on its surface (D35A and D39A) results in an increase of its stability. When two other acidic residues, Glu-76 and Glu-80, are replaced by glutamine, this does not affect the overall structure but also substantially increases the barstar stability, with a 40% increase of the free energy of folding in the latter case [35]. This suggests that some electrostatic strain destabilizes barstar. It is therefore most likely that the compensating mutations of barstar that were selected during genetic screening result from a compromise between the counter selection of additional negative charges on the surface of barstar and the affinity of barstar for the positively charged barnase.

*Acknowledgements:* We are grateful to J. Fourniat and E. Vallet for help and support during this work. We thank J. Navaza for his constant interest and for his help in molecular replacement and M. Knossow for critical reading of the manuscript. We acknowledge the staff of LURE (Orsay) for making station W32 on the Wigger line of LURE-DCI available to us. Calculations were performed on the CRAY computers at IDRIS, Orsay, France. This work was in part supported by the Grant INTAS-RFBR-95-1058.

## References

[1] Hartley, R.W. (1968) Biochemistry 7, 2401–2408.
[2] Smeaton, J.R., Elliot, W.H. and Coleman, G. (1965) Biochem. Biophys. Res. Commun. 18, 36–42.
[3] Hartley, R.W. (1993) Biochemistry 32, 5978–5984.
[4] Schreiber, G. and Fersht, A.R. (1993) Biochemistry 32, 5145–5150.
[5] Mauguen, Y., Hartley, R.W., Dodson, G., Bricogne, G., Chotia, C. and Jack, A. (1982) Nature 297, 162.
[6] Ratnaparkhi, G.S., Ramachandran, S., Udgaonkar, J.B. and Varadarajan, R. (1998) Biochemistry 37, 6958–6966.
[7] Bycroft, M., Ludvigsen, S., Fersht, A. and Poulsen, F. (1991) Biochemistry 30, 8697–8701.
[8] Lubienski, M.J., Bycroft, M., Freund, M.V. and Fersht, A.R. (1994) Biochemistry 33, 8866–8877.
[9] Guillet, V., Laphtorn, A., Hartley, R.W. and Mauguen, Y. (1993) Structure 3, 165–176.
[10] Buckle, A., Schreiber, G. and Fersht, A.R. (1994) Biochemistry 33, 8878–8889.
[11] Martin, C., Richard, V., Salem, M., Hartley, R.W. and Mauguen, Y. (1999) Acta Crystallogr. D55, 386–398.
[12] Jucovic, M. and Hartley, R.W. (1996) Proc. Natl. Acad. Sci. USA 93, 2343–2347.
[13] Jucovic, M. and Hartley, R.W. (1995) Protein Eng. 8, 497–499.
[14] Hartley, R.W. and Rogerson, D.L. (1972) Prep. Biochem. 2, 229–242.
[15] Hartley, R.W. and Rogerson, D.L. (1972) Prep. Biochem. 2, 243–250.
[16] Guillet, V., Laphtorn, A., Fourniat, J., Benoit, J.P., Hartley, R.W. and Mauguen, Y. (1993) Proteins 17, 325–328.
[17] Gill, S.C. and Von Hippel, P.H. (1989) Anal. Biochem. 182, 319–326.
[18] Raghunathan, V., Khurama, S., Gipta, V., Khurana, R., Udgaonkar, J.B. and Salunke, D.M. (1994) J. Mol. Biol. 243, 533–536.
[19] Thaller, C., Weaver, L.H., Eichele, G., Wilson, E., Karlsson, R. and Jansonius, J.N. (1981) J. Mol. Biol. 147, 465–469.
[20] Leslie, A.G.W. (1992) in: CCP4 ESF-EACMB Newsl. Protein Crystallogr., Vol. 26, pp. 27–33, SERC, Daresbury Laboratory, Warrington.
[21] Navaza, J. (1994) Acta Crystallogr. A50, 157–163.
[22] Navaza, J. and Vernoslova, E. (1995) Acta Crystallogr. A51, 445–449.
[23] Roussel, A. and Cambillau, C. (1991) TURBO-FRODO, Silicon Graphics Geometry Partner Directory, Mountain view, CA.
[24] Jones, T.A., Zhou, J.-Y., Cowan, S.W. and Kjeldgaard, M. (1991) Acta Crystallogr. A47, 110–119.
[25] Brünger, A.T. (1992) X-PLOR Manual Version 3.1, Yale University Press, New Haven, CT.
[26] Engh, R.A. and Huber, R. (1991) Acta Crystallogr. A47, 392–400.
[27] Laskowski, R.A., McArthur, M.W., Moss, D.S. and Thornton, J.M. (1993) J. Appl. Crystallogr. 26, 283–291.
[28] CCP4 (1994) Acta Crystallogr. D50, pp. 760–763.
[29] Morris, A.L., MacArthur, M.W., Hutchinson, E.G. and Thornton, J.M. (1992) Proteins 12, 345–364.
[30] Luzzati, V. (1952) Acta Crystallogr. 5, 802–810.
[31] Frisch, C., Schreiber, G. and Fersht, A.R. (1995) FEBS Lett. 370, 270–277.
[32] Schreiber, G. and Fersht, A.R. (1995) J. Mol. Biol. 248, 478–486.
[33] Meiering, E.M., Serrano, L. and Fersht, A.R. (1992) J. Mol. Biol. 255, 585–589.
[34] Kleywegt, G.J. and Jones, T.A. (1994) Acta Crystallogr. D50, 178–185.
[35] Schreiber, G., Buckle, A. and Fersht, A.R. (1994) Structure 2, 945–951.